nature energy

Article

https://doi.org/10.1038/s41560-023-01255-2

Silicon heterojunction solar cells with up to 26.81% efficiency achieved by electrically optimized nanocrystalline-silicon hole contact layers

Table of contents

Supplementary Tables

Supplementary Table 1 | The PV performance of SHJ solar cells with p-nc-Si:H HSCs .[1-5]

Parameters of HSCs	Area (cm^2)	J_{SC} (mA/cm^2)	FF (%)	V_{OC} (mV)	PCE (%)	Test centre	R_S ($\Omega \cdot cm^2$)	ρ_c ($m\Omega \cdot cm^2$)	Inst.	Ref.
4 nm p-nc-SiOx:H + 16 nm p-nc-Si:H	~3.9	38.85	80.4	719	22.47	ISFH	~0.85	~144	Delft	1
25 nm p-nc-Si:H	~4	39.48	81.4	733	23.54	AIST	-	280	AIST	2
15 nm p-nc-Si:H (Si = 56 μm)	~4	37.85	81.5	754	23.27	AIST	1.3	~130	AIST	3
p-nc-Si:H	~4	39.8	81.3	733	23.8		0.67	-	EPFL	4
p-nc-Si:H + p-nc-SiOx:H + p-nc-Si:H	~4	39.85	82.0	737.5	24.09	ISFH	~0.87	-		
27 nm p-nc-Si:H	~4	39.41	81.1	734.1	23.45	ISFH	~0.68	-	EPFL	5

Supplementary Table 2 | The PV performance of crystalline silicon solar cells in Fig. 1.[6-14]

Classification	J_{sc} (mA/cm^2)	V_{OC} (mV)	FF (%)	PCE (%)	Area (cm^2)	Test centre	Ref.
SHJ							
n-SHJ 26.8% (LONGi)	41.45	751.4	86.07	26.81	274.4	ISFH	This work
n-SHJ 26.7% (LONGi)	41.16	751.1	86.48	26.74	274.4	ISFH	This work
n-SHJ 26.5% (LONGi)	41.01	750.6	86.08	26.50	274.4	ISFH	6
n-SHJ 26.3% (LONGi)	40.49	750.2	86.59	26.30	274.3	ISFH	This work
n-SHJ 25.8% (LONGi)	40.20	750.4	85.57	25.82	274.5	ISFH	7
n-SHJ 25.3% (LONGi)	39.48	748.5	85.46	25.26	244.53	ISFH	This work
n-SHJ 25.1% (Hanergy)	39.55	747.0	84.95	25.11	244.45	ISFH	8
TOPCon							
n-TOPCon 25.2% (LONGi)	41.64	721.6	83.9	25.2	242.97	ISFH	9
n-TOPCon 25.3% (Jinko)	42.07	721.4	83.4	25.3	268.0	ISFH	10
n-TOPCon 25.8% (FhG-ISE)	42.87	724.1	83.1	25.8	4.008	FhG-ISE	11
p-TOPCon 26.0% (FhG-ISE)	42.05	732.3	84.3	26.0	4.015	FhG-ISE	12
PERC							
p-PERC 24.0% (LONGi)	41.58	694	83.3	24.0	244.59	ISFH	13
p-PERC 25.0% (UNSW)	42.70	706	82.8	25.0	4.00	Sandia	14

Supplementary Table 3| Parameters of the functional layers used for fabrication of p-a-Si:H cell and p-nc-Si:H cell in Fig. 2.

	p-a-Si:H cell	p-nc-Si:H cell
Front ESC		
Finger	45 μm width	40 μm width
TCO	150 Ω/☐	50 Ω/☐
n-nc-SiO_x:H	–	–
i-a-Si:H	–	–
Bulk		
n-c-Si	M2	M6
Rear HSC		
i-a-Si:H	–	–
p-layer	p-a-Si:H	p-nc-Si:H
TCO	80 Ω/☐	40 Ω/☐
Finger	–	–

"–" represents without change in this table.

Supplementary Table 4| Input parameters of Quokka2 simulation for p-a-Si:H cell and p-nc-Si:H cell.[15]

	p-a-Si:H cell	p-nc-Si:H cell
Unit cell dimension		
Front width (μm)	860	820
Rear width (μm)	430	410
Thickness (μm)	130	130
Bulk		
Doping type	n-type	n-type
Resistivity (Ω·cm)	1.5	1.5
τ_{SRH} (ms)	40	25
B_{rad} (cm^3/s) *	1.89×10^{-15}	1.89×10^{-15}
Auger mode	Richter 2012	Richter 2012
Front surface		
Sheet resistance (Ω/☐)	150	50
J_{01} (fA/cm^2)	1	1
Contact half width (μm)	22.5	20
Rear surface		
Sheet resistance (Ω/☐)	80	40
J_{01} (fA/cm^2)	1.2	0.5
Contact half width (μm)	45	45
Generation		
Shading width (μm)	22.5	20
Optical pathlength factor (Z)	$4n^2$	$4n^2$
Transmission	0.916	0.9383
External circuit		
Series resistance (Ω·cm^2)	0.17	0.075

* the value of B_{rad} was set as (1-0.6)×(4.73×10^{-15}), considering a photon recycling probability of ~0.6.[15]

Supplementary Table 5 | The growth recipes of the p1-p4 in Supplementary Fig. 3.

	H_2 (sccm)	SiH_4 (sccm)	B_2H_6 (2%vol in H_2) (sccm)
p1	20000	80	40
p2	20000	40	40
p3	20000	40	20
p4	20000	40	10

Supplementary Table 6 | Parameters of growth process for doped layers.

	Temperature (℃)	Pressure (mbar)	Power density (mW/cm^2)	SiH_4 flow (sccm)	H_2 flow (sccm)	B_2H_6 flow (sccm)
p-a-Si:H	170-200	0.6	38-45	240-270	300-400	100
p-nc-Si:H	170-200	3.8	185-220	30-40	14000-21000	20

Supplementary Table 7 | Input parameters of TCAD simulation used for calculating band diagrams (Fig. 3e,f) and dark *I-V* curves (Supplementary Fig. 4) of HSCs based on p-nc-Si:H and p-a-Si:H.[16-19]

Crystalline Silicon			
Model / Parameter	Simulated Model		
Bandgap narrowing	Schenk *et al.* [16]		
Mobility	Klaassen *et al.* [17]		
Intrinsic carrier density	Altermatt *et al.* [18] 9.65 × 10^9 cm^{-3} at 300 °K		
Free carrier statistics	Fermi-Dirac		
Intrinsic recombination	Richter *et al.* [19]		
SHJ contact materials & properties			
Parameter	i-a-Si:H	p-layer	TCO
Electron affinity (eV)	3.9	3.9	4.9
Band gap (eV)	1.7	1.7	3.7
Effective CB DOS (cm^{-3})	2 × 10^{20}	2 × 10^{20}	4 × 10^{20}
Effective VB DOS (cm-3)	2 × 10^{20}	2 × 10^{20}	1.3× 10^{19}
Electron/hole mobility (cm2V-1s-1)	20/4	25/5	160/40
Thickness (nm)	6	20	140
Activation energy (meV)		110.7 (p-nc-Si:H) 346.8 (p-a-Si:H)	-
Carrier Concentration (cm^{-3})			1.3x10^{20}
Tunneling mass (m_0*)	0.1	0.1	-
Urbach energy (VB tail) (meV)	50	120	-
Urbach energy (CB tail) (meV)	35	80	-
Urbach tail pre-factor($cm^{-3}eV^{-1}$)	1.88 × 10^{21}	2 × 10^{21}	-
Urbach tail e/h capture cross section (cm^2)	7 × 10^{-16}	7 × 10^{-16}	-
Gaussian peak defect density ($cm^{-3}eV^{-1}$)	1.38 × 10^{16}	1.31 × 10^{20}	-
Gaussian donor peak position (eV)	0.89	1.1	-
Gaussian acceptor peak position (eV)	1.09	1.2	-
Gaussian donor e/h capture cross section (cm^2)	3 × 10^{-14}/3 × 10^{-15}	3 × 10^{-14}/3 × 10^{-15}	-
Gaussian acceptor e/h capture cross section (cm^2)	3 × 10^{-15}/3 × 10^{-14}	3 × 10^{-15}/3× 10^{-14}	-

m_0* is electron rest mass

Supplementary Figures

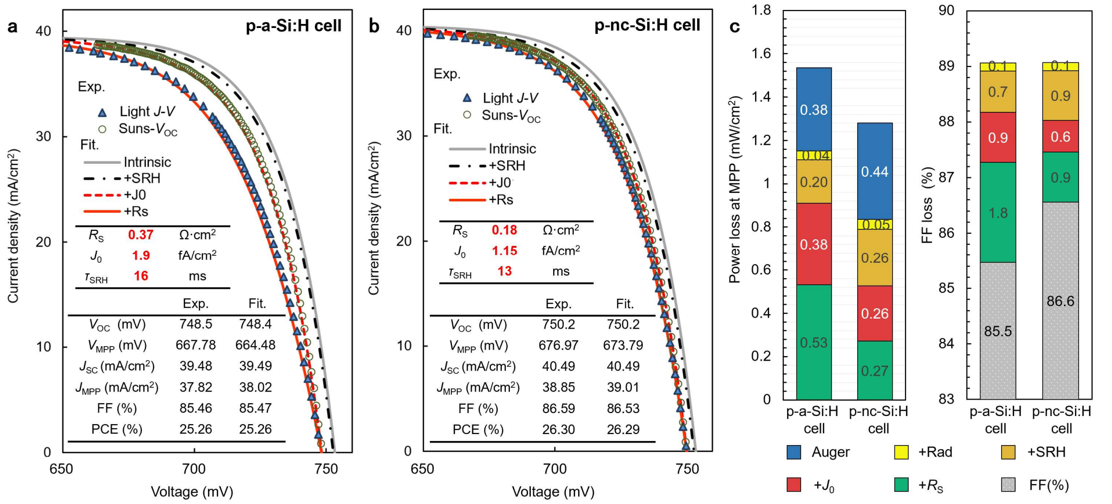

Supplementary Figure 1 | Electrical performance analysis by simple recombination model. a,b, The experimental (Exp.) and fitted (Fit.) *J-V* curves for p-a-Si:H cell (25.26%-PCE) and p-nc-Si:H cell (26.30%-PCE), respectively. Experimental curves include light *J-V* and Suns-V_{OC} curves. When fitting curves, the 'Intrinsic', '+SRH', '+J_0', and '+R_S' mean that the influence of intrinsic recombination, SRH recombination, other recombination (J_0, mainly from surface recombination)[20] and series resistance (R_S) are considered one by one in the simulation equations. Intrinsic *J-V* curves are fitted by using the equation of Auger recombination (Black *et al.*[21]) and radiative (Rad) recombination with a photon recycling of ~0.6 [15], where the wafer thickness and the doping density are set to 130 μm and 3.23×10^{15} cm^{-3}, respectively. Following the methods from ref. [22] we set τ_{SRH} =16 ms and J_0 = 1.9 fA/cm^2 (τ_{SRH} =13 ms and J_0 = 1.15 fA/cm^2) for p-a-Si:H cell (p-nc-Si:H cell) to fit the Suns-V_{OC} curves. For fitting the Light *J-V* curves, R_S of p-a-Si:H cell (p-nc-Si:H cell) is estimated as 0.37 Ω·cm^2 (0.18 Ω·cm^2). The inset tables from up to down show the fitting parameters and photovoltaic (PV) parameters, respectively. **c,** The power loss analysis (PLA) at MPP and FF loss analysis according to the fitting curves in **a** and **b**. More details are showed in Supplementary Discussion 1.

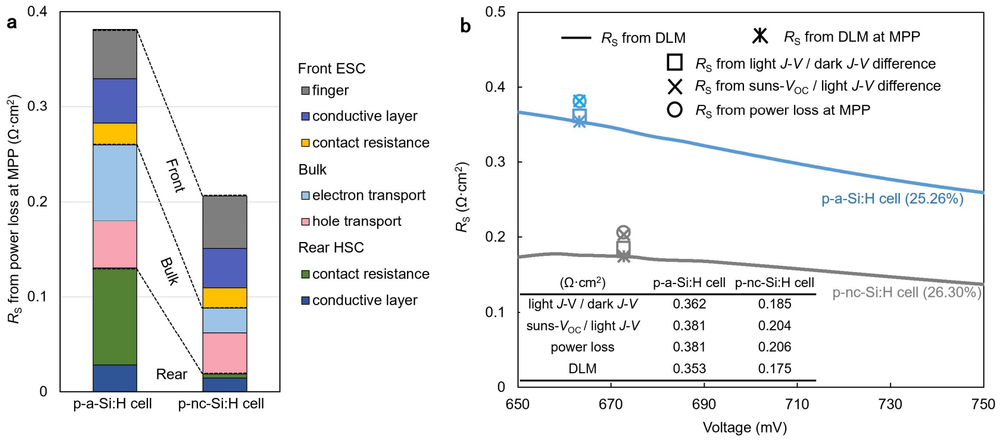

Supplementary Figure 2 | Analysis of R_S of p-a-Si:H cell and p-nc-Si:H cell. a, The R_S loss analysis derived from the fitted *J-V* curves in Figs. 2b and 2c. **b,** The extracted R_S at MPP. Four wellknown methods, 1) comparison of a one-sun with a dark *J-V* curve, 2) comparison of a Suns-V_{OC} with a one-sun *J-V* curve, 3) calculated from PLA, 4) comparison of two *J-V* curves measured at different illumination intensities (named double light method, DLM),[23] are utilized to extract R_S, as shown in the inset Table. All data are extracted from fitted *J-V* curves in Figs. 2b,c.

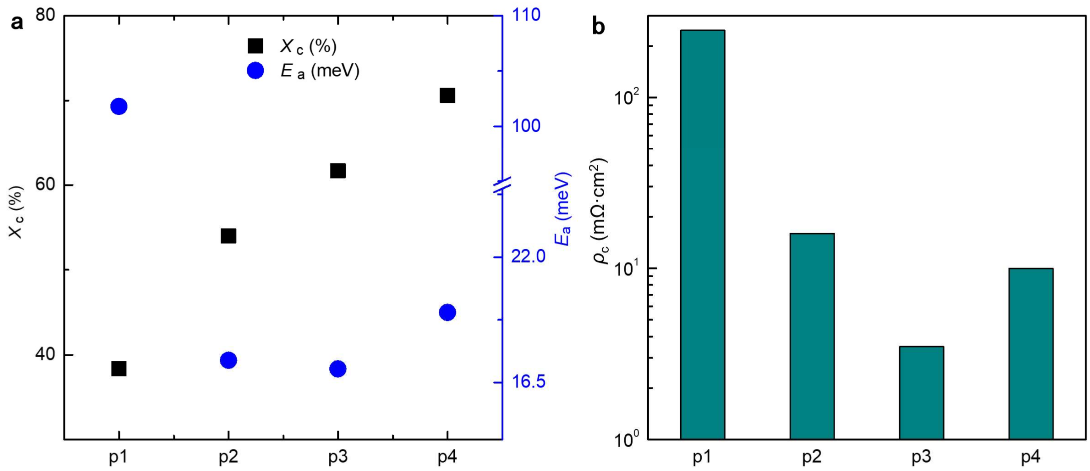

Supplementary Figure 3 | Optimization of HSCs based on p-nc-Si:H. **a,** The variation of Crystalline volume fraction (X_C) and activation energy (E_a) with the different growth recipes. **b,** The contact resistance of HSCs based on p-nc-Si:H with the different growth recipes. Here, the samples planar glass are utilized for testing E_a, and Cox and Strack method (CSM) is used to measure the contact resistances. The details of growth recipes, labeled by p1~p4 in figure, is showed in Supplementary Table 5.

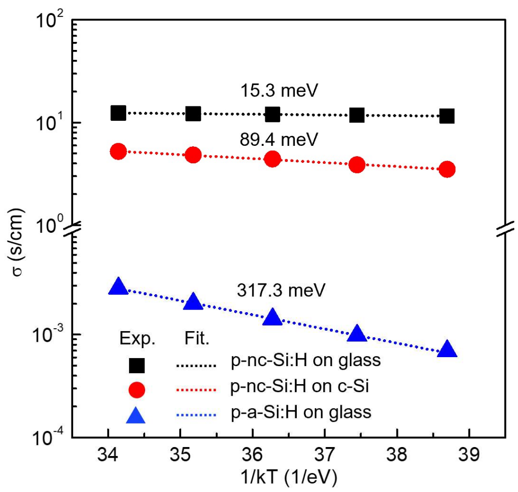

Supplementary Figure 4 | Extraction of activation energy (E_a) for p-nc-Si:H and p-a-Si:H films with light soaking. Here, the process of light soaking for testing samples was the same as that used in final solar cells. Dotted lines are the fitting curves according to the equation (2).

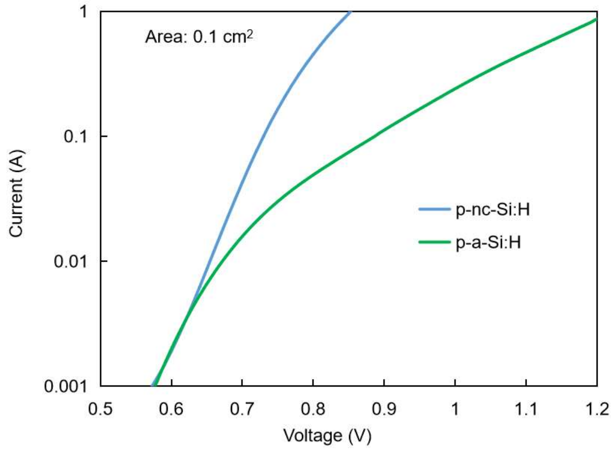

Supplementary Figure 5 | Comparison of experimental *I-V* curves for contact resistance testing devices with HSCs based on p-nc-Si:H and p-a-Si:H.

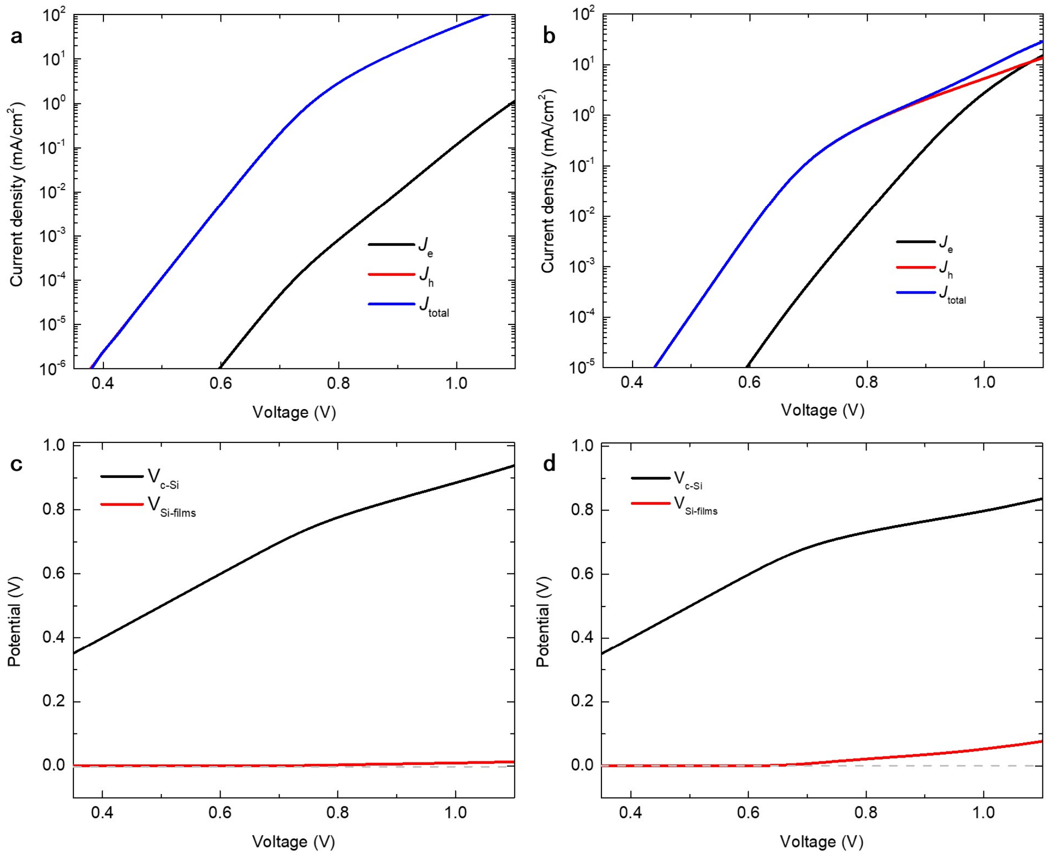

Supplementary Figure 6 | Simulated electrical results of HSCs based on p-nc-Si:H (a,c) and p-a-Si:H (b,d) from TCAD. a,b, The simulated separated *J-V* curves of contact resistance testing devices. The J_h curve (red line) and J_{total} curve (blue line) in **a** are overlapped. **c,d,** the potential drop as a function of voltage. The black lines (red lines) represent the change of potential drop on c-Si (silicon thin films) with the growth of applied voltage, while the grey dashed lines indicate the potential with 0. More details are showed in Supplementary Discussion 2.

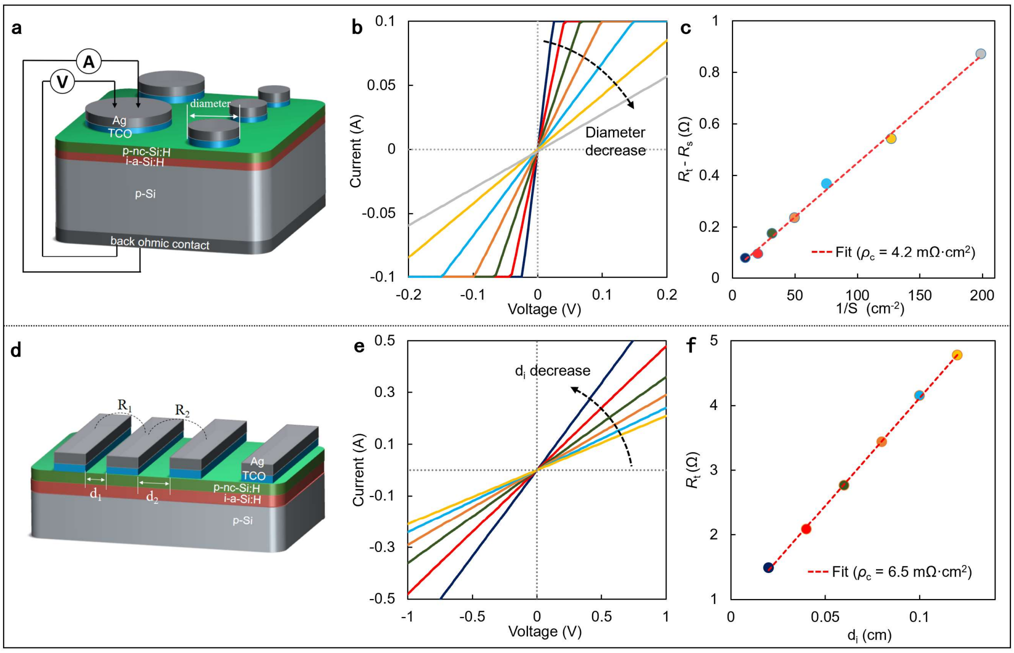

Supplementary Figure 7 | Contact resistance of HSC based on p-nc-Si:H. a-c, Cox and Strack method (CSM).[24] **d-f,** Transfer length method (TLM).[25] The testing structures are shown in **a** and **d**. The corresponding dark *I-V* curves with different diameter or different length (d_i) are shown in **b** and **e,** and then the ρ_c are extracted by the liner fittings in **c** and **f** (dashed line). It should be noted that, when the ECSM testing structure was used, the substrate of p-Si (p-type c-Si) had to be changed into n-Si (n-type c-Si) ones in **a**.

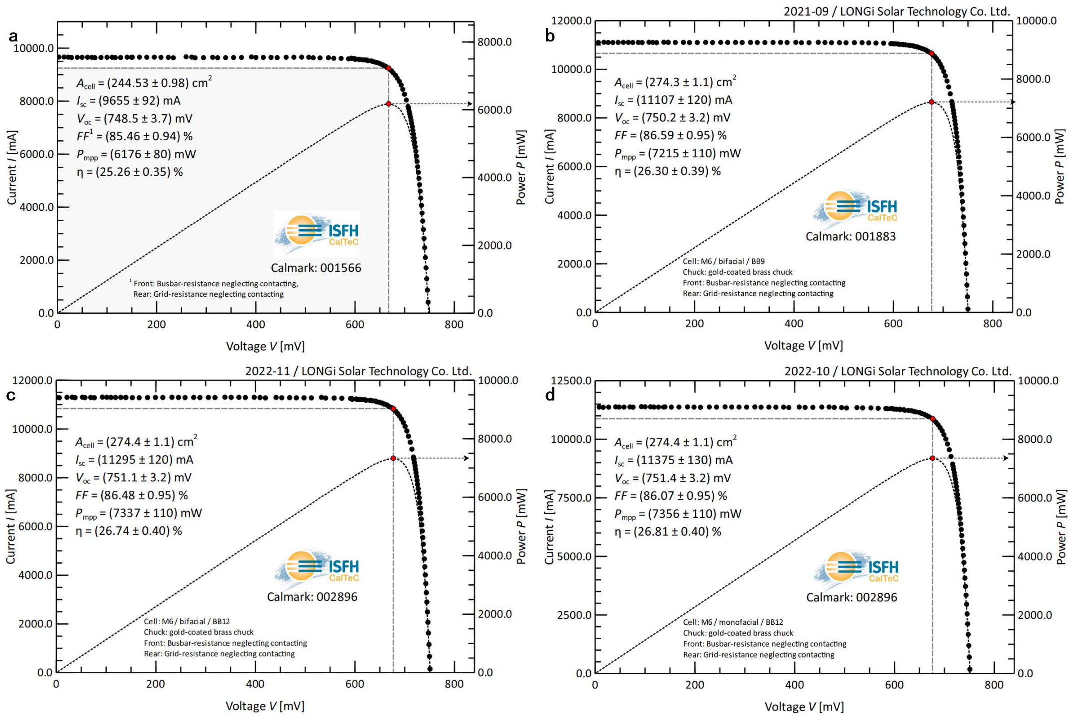

Supplementary Figure 8 | Certified results of the n-type Si solar cells with 25.26% (p-a-Si:H cell), 26.30% (p-nc-Si:H cell), 26.74% and record 26.81%-PCE.

Supplementary Discussions

Supplementary Discussion 1. Electrical performance analysis by simple recombination model

As shown in Supplementary Figures 1a and 1b, the experimental curves and the corresponding PV parameters are both highly consistent with the theoretical ones. The fitting parameters from experiments, such as R_S and J_0, are consistent with the results of Quokka simulation, proving high reliability and accuracy. Here, Auger recombination model by Black *et al.*[21] , rather than Richter' 2012 model[19] was used for simulation to avoid underestimation of SRH recombination of bulk silicon (overestimates the Auger recombination near the MPP for the doped Si substrate)[26]. According to the experiments, the wafer thickness and the doping density are set to 130 μm and 3.23×10^{15} cm^{-3}, respectively. It should mention that R_S is not a fixed value but a variable parameter changing with the applied voltage. Therefore, compensation was directly introduced according to the change of the silicon wafer conductivity that was caused by the variations in excess carrier concentration driven by applied voltages.

In contrast to the results demonstrated in Fig. 2, the information of intrinsic recombination is shown in Supplementary Figure 1c. The power loss of intrinsic recombination is close to ~0.4 mW for both cells, which is non-negligible. Due to a better evaluation of the Auger recombination by Black *et al.*, the proportion of power loss analysis (PLA) from SRH recombination increases to ~0.2 and ~0.26 mW/cm^2 for p-a-Si:H cell and p-nc-Si:H cell, respectively. The trend of other power losses is basically consistent with those in Fig. 2. To directly examine the influence of power loss on FF, the FF loss analysis is shown in the right of Supplementary Figure 1c. Obviously, the final FF is affected by recombination and R_S. The pseudo FF (pFF) contains the information from all recombination losses in absence of the effect of R_S. It is clearly seen that both cells have a nearly same pFF (at the interface of red and green squares) of about 87.3%. Of course, a slightly higher surface recombination in p-a-Si:H cell and a little bit higher SRH recombination in p-nc-Si:H cell were found, solely indicating a small variation in surface passivation and wafer quality turn by turn. Therefore, the large difference in R_S is the main reason responsible for the large difference of the final FF. In combination with the huge reduction in the R_S after nano-crystallization (Fig. 2d), it proves again that the key role of p-nc-Si:H in achieving high FF.

Supplementary Discussion 2. Simulated electrical results of HSCs based on p-a-Si:H and p-nc-Si:H from TCAD

From the comparison of Supplementary Fig. 6a,b, it can be seen that for p-nc-Si:H, the ratio of hole current/electron current at different voltages is much larger than that for p-a-Si:H. This indicates a large difference between holes and electrons density at the interface of i-a-Si:H/n-Si for HSC based on p-nc-Si:H layer. Therefore, due to the carrier population difference, the corresponding surface recombination decreases even if the defect state density remains unchanged. Of course, this can also be simply understood as the larger effective dopant density of p-nc-Si:H (lower E_a), which leads to a larger built-in potential and therefore an enhanced field passivation, thus leading to the improvement of the passivation quality. On the other hand, from the changes of hole and electron currents with voltages in TCO/p-nc-Si:H/i-a-Si:H/n-Si, the hole current is dominant in the whole voltage range. This means that the hole transport is relatively smooth with energy-less transitions. However, for the HSC based on p-a-Si:H, the electron current in the high voltage range can even exceed the hole current. It indicates that, at this voltage range, the hole transport faces energy variation crossing the HSC, which can be well confirmed from the analysis of potential drop in Supplementary Figures 6c,d. When the applied voltage was increased beyond 0.7 V, a portion of the voltage will fall on the amorphous silicon layer (p-a-Si:H/i-a-Si:H) to overcome the series resistance faced by the holes, while in p-nc-Si:H, there is almost no change. In summary, the passivation and carrier transport capability of the p-a-Si:H layer are weaker than the p-nc-Si:H counterpart, which is in accordance with the experimental results.

Supplementary References

1. Zhao, Y. *et al.* Design and optimization of hole collectors based on nc-SiOx:H for high-efficiency silicon heterojunction solar cells *Solar Energy Materials and Solar Cells* **219**, 110779 (2021).
2. Umishio, H., Sai, H., Koida, T. & Matsui, T. Nanocrystalline-silicon hole contact layers enabling efficiency improvement of silicon heterojunction solar cells: Impact of nanostructure evolution on solar cell performance. *Prog. Photovolt: Res. Appl.* **29**, 344–356 (2021).
3. Sai, H., Umishio, H. & Matsui, T. Very thin (56μm) silicon heterojunction solar cells with an efficiency of 23.3% and an open-circuit voltage of 754mV. *Solar RRL* **5**, (2021).
4. Boccard, M. *et al.* Hole-selective dront contact atack enabling 24.1%-efficient silicon heterojunction solar cells. *IEEE Journal of Photovoltaics* **11**, 9-15 (2020).
5. Fioretti, A.N., Boccard, M., Monnard, R. & Ballif, C. Low-temperature p-type microcrystalline silicon as carrier selective contact for silicon heterojunction solar cells. *IEEE Journal of Photovoltaics* **9**, 1158-1165 (2019).
6. LONGi once again sets new world record for HJT solar cell efficiency. https://www.longi.com/en/news/new-hjt-world-record/ (2022).
7. LONGi sets new world record of 25.82% for HJT solar cell efficiency. https://www.longi.com/en/news/6751/ (2021).
8. Hanergy reports 25.11% efficiency for SHJ technology. . https://taiyangnews.info/technology/hanergy-reports-25-11-efficiency-for-shj-technology/ (2019).
9. LONGi breaks three more world records for solar cell efficiency https://www.longi.com/en/news/7474/ (2021).
10. JinkoSolar: 'Record' 25.25% efficiency for TOPCon cell. https://taiyangnews.info/technology/jinkosolar-record-25-25-efficiency-for-n-type-mono-cell/ (2021).
11. Richter, A. *et al.* N-Type Si solar cells with passivating electron contact: Identifying sources for efficiency limitations by wafer thickness and resistivity variation. *Solar Energy Materials & Solar Cells* **173**, 96-105 (2017).
12. Richter, A. *et al.* Design rules for high-efficiency both-sides-contacted silicon solar cells with balanced charge carrier transport and recombination losses. *Nature Energy* **6**, (2021).
13. Wang, Q. Status of crystalline silicon PERC solar cells. . in *NIST/UL Workshop on Photovoltaic Materials Durability* (Gaithersburg, MD USA, 2019).
14. Green, M.A. The passivated emitter and rear cell (PERC): From conception to mass

production. . *Sol Energy Mater Sol Cells* **143** 190-197 (2015).
15. Richter, A., Hermle, M. & Glunz, S.W. Reassessment of the Limiting Efficiency for Crystalline Silicon Solar Cells. *IEEE Journal of Photovoltaics* **3**, 1184-1191 (2013).
16. Schenk, A. Finite-temperature full random-phase approximation model of band gap narrowing for silicon device simulation. *Journal of Applied Physics* **84**, 3684-3695 (1998).
17. Klaassen, D. A unified mobility model for device simulation—II. Temperature dependence of carrier mobility and lifetime. *Solid-State Electronics* **35**, 961-967 (1992).
18. Altermatt, P.P., Schenk, A., Schmithusen, B. & Heiser, G. A simulation model for the density of states and for incomplete ionization in crystalline silicon. I. Establishing the model in Si:P. *Journal of Applied Physics* **100**, 113714 (2006).
19. Richter, A., Werner, F., Cuevas, A., Schmidt, J. & Glunz, S.W. Improved parameterization of Auger recombination in silicon. *Energy Procedia* **27**, 88-94 (2012).
20. Cuevas, A. & Macdonald, D. Measuring and interpreting the lifetime of silicon wafers. *Solar Energy* **76**, 255-262 (2004).
21. Black, L.E. & Macdonald, D.H. On the quantification of Auger recombination in crystalline silicon. *Solar Energy Materials and Solar Cells* **234**, 111428 (2022).
22. Yoshikawa, K. *et al.* Silicon heterojunction solar cell with interdigitated back contacts for a photoconversion efficiency over 26%. *Nature Energy* **2**, 17032 (2017).
23. Pysch, D., Mette, A. & Glunz, S.W. A review and comparison of different methods to determine the series resistance of solar cells. *Solar Energy Materials & Solar Cells* **91**, 1698-1706 (2007).
24. Cox, R.H. & Strack, H.A. Ohmic contacts for GaAs devices. *Solid State Electronics* **10**, 1213-1218 (1966).
25. Reeves, G.K. & Harrison, H.B. Obtaining the specific contact resistance from transmission line model measurements. *IEEE Electron Device Letters* **3**, 111-113 (2005).
26. Niewelt, T. *et al.* Reassessment of the intrinsic bulk recombination in crystalline silicon. *Solar Energy Materials and Solar Cells* **235**, 111467 (2022).